Applied Thermal Engineering 254 (2024) 123913

Contents lists available at ScienceDirect

Applied Thermal Engineering

journal homepage: www.elsevier.com/locate/apthermeng

Research Paper

Experimental investigation of a transcritical CO_2 refrigeration system incorporating rotary gas pressure exchanger and low lift ejectors

Muhammad Zahid Saeed [a,*], Azam Thatte [b], Krzysztof Banasiak [c], Armin Hafner [a,*], Ángel Álvarez Pardiñas [d]

[a] NTNU, Department of Energy and Process Engineering, Kolbjørn Hejes vei 1B 7491, Trondheim, Norway
[b] Energy Recovery, San Leandro, CA 94577, USA
[c] SINTEF Energy Research, Sem Sælands vei 11 7034, Trondheim, Norway
[d] Energy Division, Galicia Institute of Technology ITG, 15003 A, Coruña, Spain

ARTICLE INFO

Keywords:
Rotary gas pressure exchanger
Carbon dioxide
R744
Refrigeration
Ejector
Expansion work recovery
Energy efficiency

ABSTRACT

Natural refrigerants like CO_2 are playing a significant role in making refrigeration and heat pump systems climate-friendly by slowly phasing out the high global warming refrigerants like hydrofluorocarbons (HFCs). However, the efficiency of a transcritical CO_2 refrigeration system declines significantly when the ambient temperature increases, primarily attributed to the high-pressure lift and the losses incurred during expansion. To remedy this issue, this paper presents a novel rotary gas pressure exchanger (PXG) device, which simultaneously achieves high differential pressure expansion work recovery and the "free compression" of the portion of the flash gas in a compact, rotary machine. For this, a PXG device is designed, fabricated, and tested to achieve free compression of CO_2 over the entire differential pressure of approximately 70 bar between a receiver and a gas cooler. This is one of the highest free-pressure lift provided by any device to date in CO_2 refrigeration. However, there is a small pressure loss of approximately 1–2 bar in the system due to viscous and inertia losses in the piping and in the PXG itself, which needs to be overcome by an external booster device. Results on a baseline PXG integrated system with two low lift booster compressors are presented, which show up to 60 bar free pressure lift and up to 18.2 % COP improvement provided by PXG. Additionally, key performance characteristics of the PXG, like the expansion work recovery, the mass boost ratio, direct fluid-to-fluid contact, and no pass-through operation are experimentally quantified. This work also presents a novel method to integrate two low lift ejectors with PXG to eliminate the need for separate low lift compressors. The low lift ejectors are designed, fabricated, and tested in-house, followed by their integration with the PXG device. A new type of transcritical CO_2 refrigeration system is designed to integrate these low lift ejectors with PXG, and experiments are conducted at various evaporator thermal duties and gas cooler exit temperatures, simulating varying ambient temperature conditions. A novel control system to control the gas cooler pressure to optimal thermodynamic levels using PXG rotational speed is demonstrated experimentally. Further, automated control of high-pressure low lift ejector mass flow using an in-built needle design has been successfully demonstrated to optimise PXG mass boost performance. The LP low lift ejector achieved a successful pressure lift of 3.8 bar, and the HP low lift ejector showed a lift of 5.7 bar on the top of 42 bar free pressure lift provided by PXG for up to 5.8 kg/min mass flow delivered by free PXG compression. The results from this study demonstrate that the PXG device provides a significant energy efficiency improvement to the transcritical CO_2 refrigeration system, and the novel low lift ejectors, when integrated with PXG, provide a successful method to maximise PXG's thermodynamic potential.

1. Introduction

CO_2 is one of the best alternative refrigerants to many synthetic HFCs that will experience phase-out in the short and medium term due to the existing and upcoming environmental regulations. CO_2 is a long-term solution due to its low global warming potential and zero ozone depletion potential [1,2]. CO_2 refrigeration units and heat pumps are

* Corresponding authors.
E-mail addresses: muhammad.z.saeed@ntnu.no (M. Zahid Saeed), athatte@energyrecovery.com (A. Thatte), krzysztof.banasiak@sintef.no (K. Banasiak), armin.hafner@ntnu.no (A. Hafner), aalvarez@itg.es (Á. Álvarez Pardiñas).

https://doi.org/10.1016/j.applthermaleng.2024.123913
Received 15 January 2024; Received in revised form 26 May 2024; Accepted 9 July 2024
Available online 11 July 2024

Nomenclature

Aux	Auxiliary
COP	Coefficient of performance
Com	compressor
DP	Differential pressure
EJ	Ejector
ERI	Energy recovery international
EVAP	Evaporator
FGBV	Flash gas bypass valve
GC	Gas cooler
HFCs	Hydrofluorocarbons
HP	High pressure
HPTD	High pressure travel distance
IHX	Internal heat exchanger
LT	Low temperature
LP	Low pressure
LPTD	Low pressure travel distance
LIQ	Liquid
MBR	Mass boost ratio
MT	Medium temperature
PXG	Pressure exchanger
P	pressure (bar)
PAR	Parallel
SEP	Separator
s	supercritical
Temp	Temperature (℃)
T	Temperature (℃)
VSD	Variable speed drive

Subscripts

in	inlet
out	outlet

competitive choice due to non-toxicity, non-flammability, compactness, high heat transfer and volumetric refrigeration capacity [3–8]. New CO_2 systems benefit greatly from having all thermal functions (cooling and heating) in one unit with reasonable space savings [9].

Enhancing system energy efficiency stands out as the most effective and economical approach, with the saved energy directly translating into emission reductions [10]. Energy efficiency in CO_2 refrigeration systems is significantly affected at higher ambient temperatures. Due to the low critical temperature of CO_2, systems operate in transcritical mode in warm climates. In transcritical operation, the throttling loss is higher than in traditionally employed synthetic refrigerants because of the high-pressure difference between heat rejection and absorption. In transcritical operation, the expansion happens from supercritical to the two-phase region, and high throttling loss leads to higher vapour quality, which can reduce evaporation capacity [11–13].

Researchers have conducted extensive theoretical and experimental studies to improve the performance of "CO_2 only" refrigeration systems at all environmental conditions [14,15]. The 1st generation CO_2 booster system is a standard solution for refrigeration systems in many countries and is successful in countries with cold and mild weather [9,16]. A 2nd generation CO_2 system, i.e., parallel compression, came up after the scientific developments, and the experimental results show that it can give 5 % higher performance in warm climates and 3.65 % for moderate climates compared to a standard booster system [17]. Purohit et al. [18] investigated five different configurations of booster and parallel systems and highlighted the energy and economic savings of the best configuration according to the climatic conditions of different cities. Fricke et al. [19] investigated a laboratory-scale CO_2 system with LT (9.1 kW at −30 °C) and MT (34 kW at −6.7 °C) evaporation and reported the COP of 2.2 at an ambient temperature of 32.2 °C. Wang et al. [20] studied parallel compression for supermarket refrigeration with a sub-cooler. They reported a 6.8 % average increase in seasonal energy efficiency ratio compared to a system without a sub-cooler.

The 3rd generation CO_2 system, i.e., ejector-supported system, is an advanced system with high performance. Lee et al. [21] experimentally evaluated the CO_2 air conditioning system using an ejector, including an internal heat exchanger. They investigated the motive nozzle throat diameter and distance between the nozzle and diffuser. Their results show a COP improvement of 15 % compared to the conventional system under the given conditions. Xu et al. [22] experimentally evaluated the ejector efficiency of the transcritical system and concluded that the efficiency is mainly within the range of 20 % to 30 %. Li et al. [23] investigated the transcritical CO_2 ejector system and found that the COP can be improved by 16 % compared to the basic cycle. Banasiak et al. [24] investigated the multi-ejector block with four cartridges in parallel as a replacement for a high-pressure expansion valve. Their experimental results showed ejector performance higher than 30 % for a broad range. The ejector is sensitive to operating parameters, and the off-design performance is crucial in real applications. The efficiency and the entrainment ratio are key factors in CO_2 ejector systems [12]. Qin et al. [25] investigated the novel approach to the ejector cycle with two evaporators and reported the combined (heating and cooling) COP of 11 at their specified conditions. The complex geometries of single and multi-phase ejectors and their effect on the performance of various applications are widely discussed in the literature [26–30]. The current work is limited to experimental validation and cycle performance, so the discussions about these geometries are not included. An expansion turbine is another option that can improve the system performance between 14 % to 17 % by recovering the expansion work [31]. Mechanical sub-cooling and evaporative cooling are two options that enhance the gas cooling process and improve system efficiency in warmer regions. In addition, consolidating all thermal functions in one compact CO_2 unit can enhance the performance and reduce the investment [9].

The research on technologies that improve the performance of CO_2 systems under high ambient temperature conditions is ongoing. The latest development is the rotary gas pressure exchanger (PXG), an efficiency-enhancement device. The literature on PXG is limited and primarily published by the same authors of this work [32–37]. Most of this theoretical literature is rediscussed here as well, but with an addition of experimental results. The PXG achieves expansion work recovery by expanding the high-pressure supercritical CO_2 from the gas cooler/condenser exit to the low pressure in high-speed rotary ducts through an "isentropic" like process and using the enthalpy change extracted during this expansion process to perform the work of compression on the low-pressure gaseous CO_2. During the compression process, the low-pressure flash gas is brought into direct contact with high-pressure supercritical CO_2, thus creating an acoustic wave that propagates through the rotary duct, which compresses the low-pressure flash gas to the same pressure as the high-pressure supercritical CO_2. This avoids the need for any external mechanical or electrical energy input (e.g., external compressor driven by motor) to achieve this compression. The mass flow compressed by PXG is proportional to the density ratio between its low-pressure inlet stream and the high-pressure inlet stream. Due to this, PXG can compress only a certain fraction of the total system mass flow using such "free" compression and thus, the main compressor for the refrigeration system is still required to compress the remaining flow. However, due to this "free compression", PXG can reduce the compression work of the main compressor and improve the system's energy efficiency. The fundamental gas dynamics, mass transport and thermal transport taking place inside PXG and its operation in a

refrigeration cycle have been described by the authors previously [32–37]. Fig. 1 shows the geometry of the PXG device. PXG consists of a high-speed axially ducted rotor with cylindrical ducts distributed around its axis of rotation. The rotor is situated between two stator end caps at its axially opposite ends. Each end cap has an inlet and an exit port. The high-pressure inlet (HP_{in}) port and low-pressure exit (LP_{out}) port are located on the same end cap on one side of the rotor, while the low-pressure inlet (LP_{in}) port and high-pressure exit (HP_{out}) port are on the second end cap on the axially opposite end of the rotor. High-pressure supercritical CO_2 from the gas cooler exit enters through the HP_{in} port, expands via an isentropic-like expansion process (as opposed to the isenthalpic expansion across a high-pressure transcritical valve (HPV) and leaves through the LP_{out} port as a low-pressure cold two-phase liquid gas CO_2 mixture. The two-phase flow exiting the LP_{out} port then proceeds to the liquid receiver (flash tank) of the refrigeration system. The high-pressure supercritical CO_2 entering the HP_{in} port proceeds to fill the rotor duct that is exposed to the HP_{in} port and travels a certain axial distance along the length of the duct. This distance, when normalised by the length of the duct, is termed "HP_{in} Travel Distance" ($HP_{in}TD$) and can be calculated by taking the ratio of volumetric flow entering the HPin port to the product of total rotor duct volume and rotational speed. $HP_{in}TD$ is maintained just a little less than 100 % so as to maximise the available volumetric capacity of the rotor but at the same time to make sure that this HPin flow does not exit through HP_{out} port at the axially opposite end (since HP_{out} port will also be exposed to the same duct at the same time). This helps ensure avoid "pass-through" of cooler high-pressure supercritical HP_{in} flow to hotter high-pressure supercritical HPout flow. The incoming HP_{in} flow rather displaces the compressed HP_{out} flow that had occupied this same duct volume previously and helps drive the compressed HP_{out} plug of fluid out of the duct as if it's a virtual piston. The HPin fluid now fills the duct, and as the rotor continues its rotation, it gets sealed in the land area of the end cap face between the inlet and exit ports. As the duct continues rotation further, this duct gets exposed to the low-pressure LP_{out} port, and an expansion wave propagates through the duct and the high-pressure supercritical plug of fluid in the duct expands through LP_{out} and converts into a cold two-phase liquid gas mixture through an "isentropic-like" expansion process. Since this process is more efficient than isenthalpic expansion through an HPV, it produces more liquid mass fraction after expansion than what an HPV would produce. Thus, more liquid mass flow is produced in the receiver per unit total system mass flow. Since the higher the liquid mass fraction, the lower the total system mass flow required for a given evaporator load, the efficiency of the system increases due to the PXG expansion process. This is only one smaller part of the benefit provided by the PXG. The larger benefit of PXG actually comes from "free compression" that it provides during the second half of its rotation cycle, which is discussed next.

During the above process of expansion, as the duct expands its fluid plug through the LP_{out} port, the LP_{in} port also gets exposed to the duct, and the low-pressure flash gas from the receiver enters the duct from the axially opposite end of the duct. This incoming low-pressure flash gas from the receiver drives the now expanded plug of fluid through LP_{out} port and occupies its place instead. The flash gas fills the duct up to a certain length of the duct. This length, when normalised by the total length of the duct, is termed "LP_{in} Travel Distance" ($LP_{in}TD$). $LP_{in}TD$ can be calculated as the ratio of the volumetric flow entering LP_{in} port to the product of total duct volume and its rotational speed. $LP_{in}TD$ is maintained just a little less than 100 % to ensure none of the flash gas entering LP_{in} port leaves through the LPout port. This is carefully adjusted using the LP_{in} volumetric flow rate. The low-pressure LP_{in} fluid filled duct then continues its rotation and gets sealed in the land area of the end cap between the inlet and exit ports. As the duct continues its rotation, it gets exposed to the high-pressure HP_{out} port, and a compression wave propagates through the duct, thus compressing the low-pressure duct fluid to the high pressure (almost the same pressure as the gas cooler pressure). In the process, its temperature also increases due to compression. The specific differential enthalpy (specific work) required for this compression is extracted through the expansion process described earlier. However, the mass flow compressed is only a fraction (ranging from ~ 10 % to ~ 35 %) of the mass flow expanded (due to the density ratio mentioned earlier) depending on the thermodynamic state of the HP_{in} fluid stream (i.e. gas cooler exit). The now compressed plug

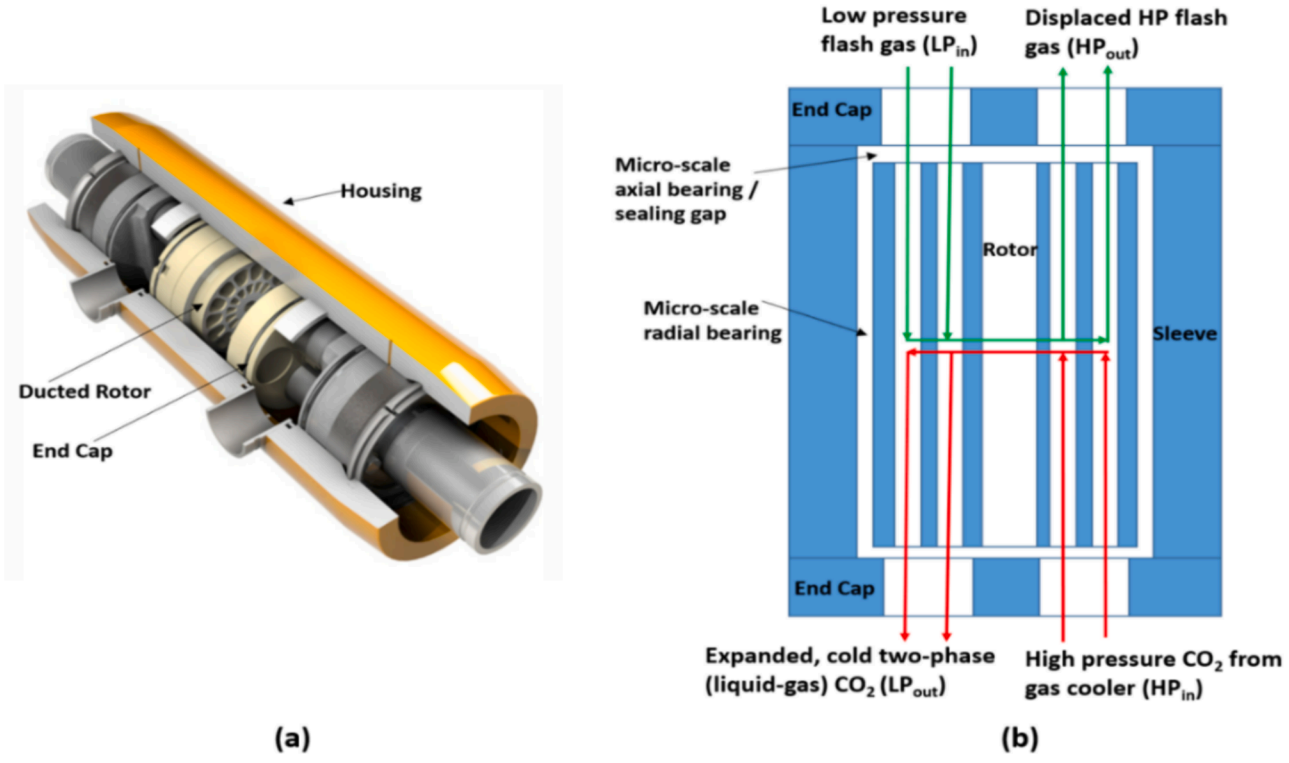

Fig. 1. PXG internal mechanism (a) 3D cut section (b) Four ports of the PXG.

of fluid in the duct gets expelled from the duct by the incoming HP_{in} fluid stream as the HP_{in} port also gets exposed to the duct from the axially opposite end during its transit across the HP_{out} port. This high-pressure, hotter supercritical HP_{out} fluid then proceeds to the gas cooler inlet and merges with the compressor discharge fluid stream. A small pressure drop (~1–2 bar) takes place in the PXG and in the piping, and to overcome this small pressure drop, the LP and HP ejectors are used, as described in the later part of this paper. The HP_{in} and LP_{in} inlet ports have aerodynamic passages designed to induce swirl into the flow as the flows enter through them. This produces an aerodynamic torque on the rotor that creates a self-sustaining rotary motion without needing an external motor.

Fig. 2 shows the four stages of the PXG operation. In stage 1, the low-pressure flash gas from the liquid receiver tank enters the PXG through the LP_{in} port and fills the duct dictated by low-pressure travel distance ($LP_{in}TD$). The non-dimensional travel distance depends on the rotational speed, rotor duct volume and the volumetric flow rate. The LP_{in} flow pushes the LP_{out} flow from the previous cycle. In the buffer zone, the two fluids can mix. However, it will remain within the duct by design. The two fluids get sealed (stage 2) as the duct rotates. When the duct is just exposed to the HP_{in} port, the generated pressure wave pressurises the LP_{in} stream to the HP_{in} pressure level with some isentropic efficiency. The LP_{in} density increases and occupies reduced volume with a constant mass in the duct. In stage 2.5, heat exchange happens from the hot to cold stream at a rate that depends on the density, thermal conductivity, heat transfer coefficient, specific heat capacity and, more importantly, the available time (rotational speed) before the next stage. In stage 3, the duct is completely aligned with HP_{in} and HP_{out} ports. The flow from the exit of the gas cooler enters through the HP_{in} port and occupies the duct dictated by the HP travel distance. As HP_{in} enters, it pushes the LP_{in} (now HP_{out}) out of the duct with the same volumetric flow rate.

The density of HP_{out} is different from HP_{in} and LP_{in}, and it dictates the flow out in the supercritical state. The duct continues rotation, and stage 4 begins. The duct is sealed again at this stage, but this time at high pressure. When the duct is just exposed to LP_{in} and LP_{out}, an expansion wave sets and reduces the duct pressure with some isentropic efficiency. Due to this expansion wave, the s-CO_2 HP_{in} flow changes its state to low-pressure two-phase CO_2. The vapour quality of the LP_{out} depends on the isentropic efficiency. In stage 4.5, two-phase CO_2 then exchanges heat for a few milliseconds with LP_{in} and may vaporise a very small fraction of LP_{out} stream. This two-phase CO_2 goes out through the LP_{out} port and flows to the liquid receiver tank [33–35].

The present work shows the first experimental result of a novel method to combine PXG with the two in-house designed and fabricated low differential pressure ejectors to increase system efficiency and reduce complexity. While PXG provides "free compression" over a large differential pressure (of the order of ~ 60–70 bar), in the absence of low differential pressure boost ejectors, the system would have required a low DP boost device (e.g. a boost compressor) to overcome ~ 1–2 bar differential pressure loss in the piping and inside PXG. Such boost compressors also typically require oil management and oil separation systems that add cost and complexity. The novelty of the current work is the design, fabrication, integration and testing of two low DP ejectors integrated with PXG. Another novelty presented in this paper is the automated control of the HP ejector flow using a novel needle design that facilitates maximum utilisation of PXG potential. In addition, the experimental results for the previous approach of using two small booster compressors to integrate PXG are also discussed. The new innovative system layout was conceived to simplify the state-of-the-art solutions to integrate PXG into the CO_2 refrigeration systems. The proposed configuration's operational characteristics, viability, and conceptual framework are verified across various operating conditions.

2. Experimental test facility

The experimental test facility, known as SuperSmart-Rack, located at the NTNU/SINTEF laboratory, is a multipurpose testing facility specifically built to emulate medium-sized supermarkets. The system has the capability to generate cooling at three distinct temperature levels, namely those corresponding to medium temperature (MT), low temperature (LT), and air conditioning applications.

Fig. 3 shows the system's simplified process and instrumentation diagram (P&ID), omitting those components irrelevant to the PXG-configuration test campaign. The PXG system depicted in Fig. 3 consists of two compressor groups: MT compressors and parallel (Par) compressors. Each compressor group initially consists of three compressors (Table 1), but this can be adjusted depending on the test campaign and experimental conditions with a system of valves located upstream of several compressors. The system has three gas coolers (GC), with heat rejection facilitated by an auxiliary loop of glycol, water, and CO_2. The expansion of a high-pressure stream can occur in two distinct components, namely the high-pressure control valve (HPV) and the PXG. The two refrigerant accumulation tanks are the liquid receiver and the liquid separator. The MT evaporators can emulate the cooling need at the set point temperature. Utilising internal heat exchangers (IHX 1 and IHX 2) guarantees the attainment of superheat conditions for the suction stream of compressors. For the current experimental investigations, there was no refrigerant flow on the cold side of the first heat exchanger (IHX 1).

The facility has a high degree of flexibility and has been used in the past for testing various configurations and components [38,39]. The PXG setup is an addition that is integrated into the main system, with a total of five connection points and two ejectors (See Fig. 4) . Two connections are located on the high-pressure side, upstream (Point 2) and

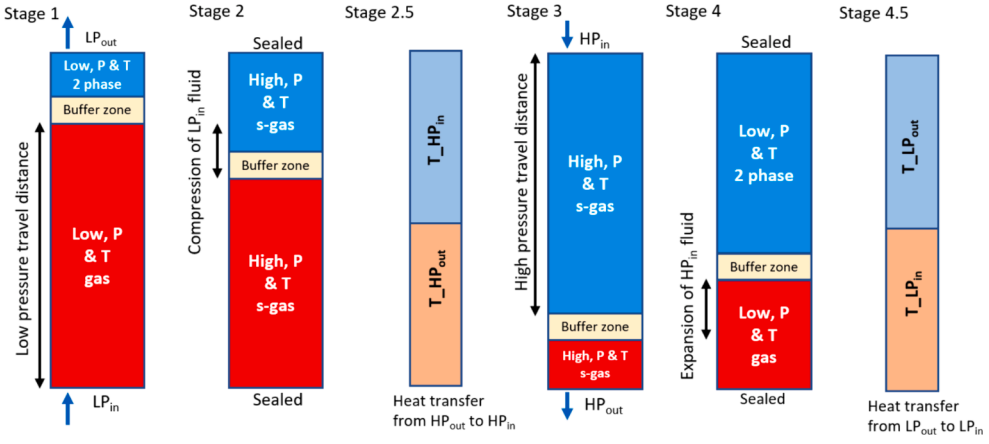

Fig. 2. Different stages of compression, expansion, and heat transfer.

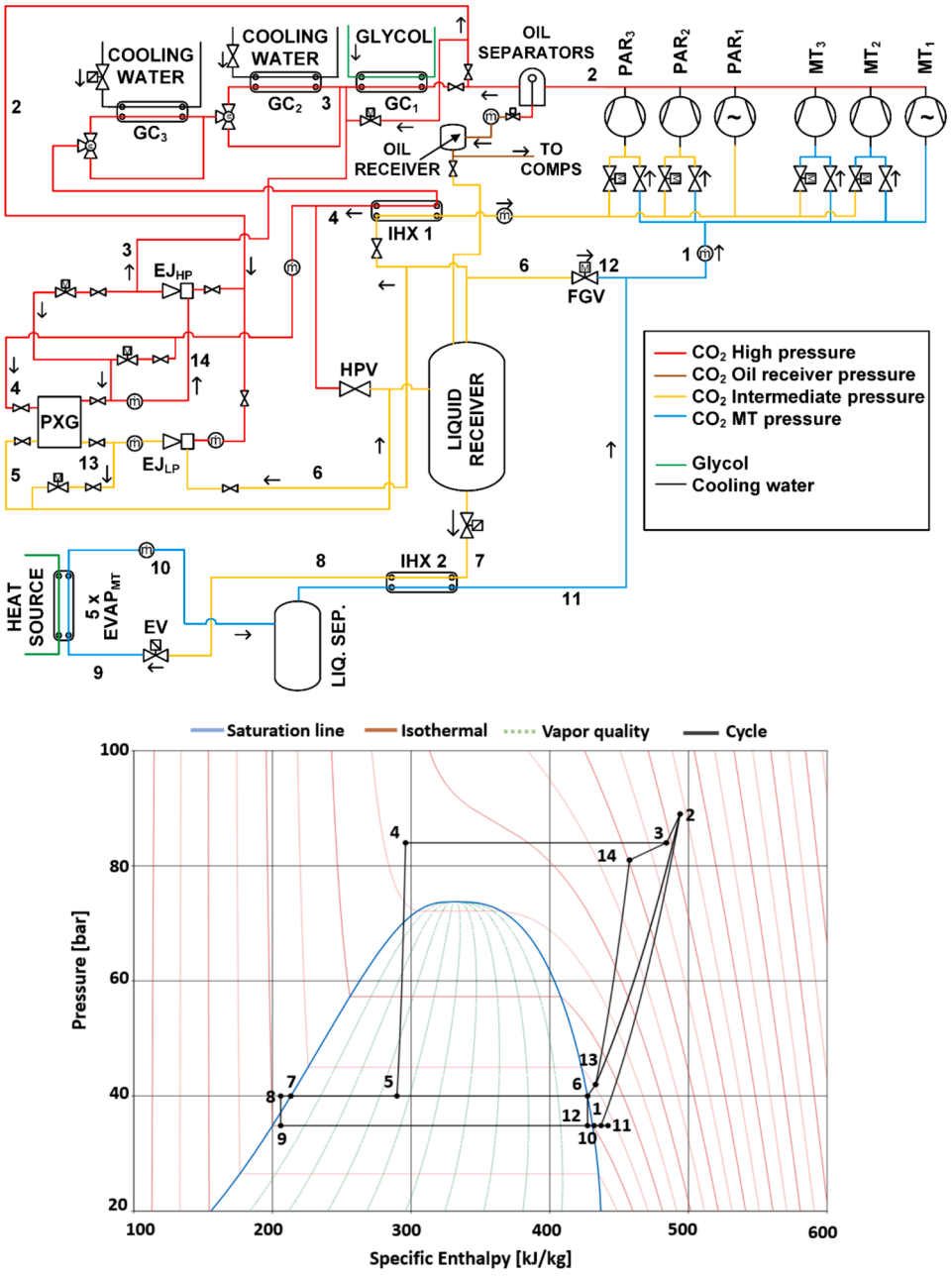

Fig. 3. PXG configuration P&ID and Ph diagram.

Table 1
Compressors installed in the experimental setup.

Compressor group	Model (Bitzer)	Displacement (m^3/h)
MT	4 MTC-10 K-40S	6.5 (VSD)
	4 MTC-10 K-40S	6.5 (VSD)
	4 JTC-15 K-40P	9.2
Parallel	2 KTE −7K-40S	4.8 (VSD)
	2 KTE −7K-40S	4.8 (VSD)
	4 JTC-15 K-40S	9.2

downstream (Point 3) of GC_1. These two connections manage the ejector's motive (point 2) and the outlet flow (point 3) of the high-pressure ejector (EJ_{HP}). The third connection (point 4) downstream of IHX 1 is directed at PXG HP_{in}. The fourth (Point 6) and fifth (point 5 after HPV) connections near the liquid receiver are intended to deal with flash gas (LP ejector suction) and two-phase CO_2 (PXG LP_{out}).

The system includes the two ejectors, namely the EJ_{LP} and EJ_{HP}, and the PXG and auxiliary components like temperature and pressure sensors and flow meters. A pressure increase (point 6 to 13) is necessary to facilitate the entry of flash gas from the liquid receiver tank into the PXG, which is attained with the low-pressure ejector (EJ_{LP}). Following the compression of flash gas (Point 13 to 14) to high pressure in PXG, a further increase in pressure (Point 14 to 3) is necessary to get the desired gas cooler pressure provided by the HP ejector (EJ_{HP}). These LP and HP ejectors or booster compressors are essential for this configuration to overcome pressure losses [35] and to push the streams in and out of PXG. The motive flow for both ejectors is obtained from the compressor discharge line (Point 2). To achieve operational functionality, it is imperative that the pressure at the discharge of the compressor (Point 2) must be higher than the GC pressure (Point 3). This pressure difference depends on the efficiency of the ejectors, with particular emphasis on the high-pressure (HP) ejector. The geometry of the LP ejector is fixed, but the HP ejector has a motorised control system to regulate the motive

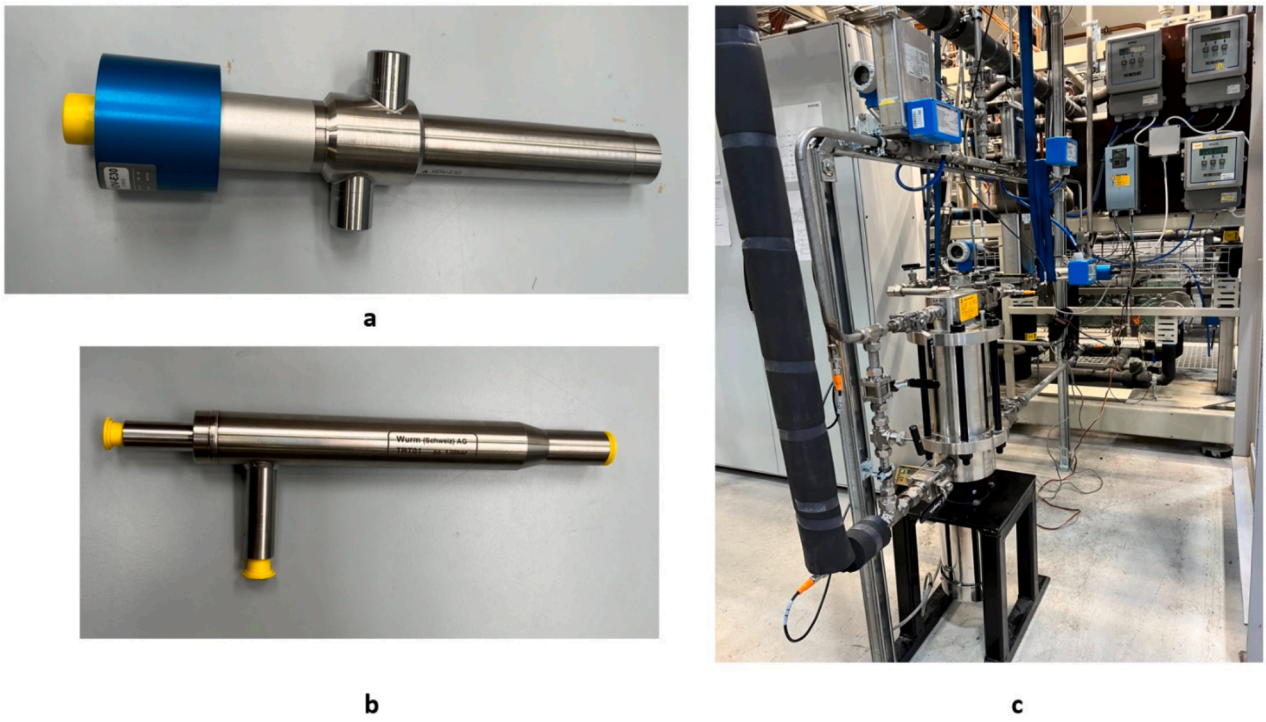

Fig. 4. Experimental setup (a) HP ejector (b) LP ejector (c) PXG add-on.

flow. HP ejector motive nozzle and the metering valve (bypassing GC_1) dictate the compressor discharge pressure.

The amount of flash gas lifted by the LP ejector is determined from the two flow meters upstream and downstream of the LP ejector. After lifting this flash gas, it is directed towards PXG HP_{in} (Point 13). The flow rate of flash gas removal from the PXG HP_{out} (Point 14) is given by the flow meter on the line. The HP ejector then lifted the flash gas (Point 14) to GC pressure (point 3) and delivered this to GC_2. At GC_2, the flow rate is the sum of LP ejector motive and suction, HP ejector motive, and any extra flow that arrived through HP ejector suction due to leaking within PXG. This combined flow rejected heat in GC_2 and maintained the GC outlet temperature as requested. This flow then entered through the HP_{in} port (point 4) of PXG and left the PXG through the LP_{out} port (Point 5) as a low-pressure two-phase flow. The PXG motor regulates and maintains the desired GC pressure, equivalent to the HPV with other system configurations. It controls the speed of the PXG rotor and acts more as a regenerative brake than a motor.

For accurate validation, it is essential that the system operates under steady-state conditions for a specified period. For our experiments, a minimum duration of 10 min of steady-state operation is required. Maintaining this steady state involves carefully controlling the heat load and sink factors at the predetermined pressure and temperature levels. The experiments were performed for four GC outlet temperatures of 33 °C, 35 °C, 37 °C and 38 °C, liquid receiver pressure around 40 bar, evaporation temperature 0 °C and evaporation capacity of 70 kW.

2.1. Data acquisition and uncertainty

The experimental equipment was monitored and controlled using a commercial controller (Danfoss AK-PC 728A) and software to modify the CO_2 cycle set points. A distinct LabVIEW programme regulated the secondary system, including pumps and valves of the glycol and water loop. The LabVIEW programme used a PID controller to regulate the PXG motor RPM, ensuring the GC pressure remained at the designated GC temperature, while the HPV was only operated as a safety device, being kept closed during the experiments. To ensure that the flow is directed through PXG rather than HPV, the set point for the PXG motor was adjusted to be 2 bar lower than the optimised GC curve. The decrease in the set point of PXG resulted in the HPV opening at 0 %. From a commercial standpoint, it may be advantageous to adjust the HPV setting to a higher value and allow PXG to function on an optimised GC curve. Table 2 shows the measuring devices utilised in experiments, together with their respective levels of accuracy.

The average measurement uncertainties observed through the experimental campaign, considering the accuracies of the sensors as well as the variations from the steady state over time, are shown in Table 3. The LP and HP ejector performance was evaluated with specific entropy and specific enthalpy values, which are determined by input temperature and pressure measurements. The thermodynamic properties were determined by utilising the REFPROP 10 database [40]. In order to account for the uncertainty related to these properties, a methodology described by Apera et al. [41] was used. The methodology incorporated the fluctuations in thermodynamic properties arising from the uncertainty associated with each parameter employed in its calculation.

Table 2
Data acquisition equipment and their indicated accuracy.

Component	Model	Producer	Indicated accuracy
Absolute pressure transmitter	Cerabar S PMP21	Endress + Hauser	± 0.3 % of set span
Differential pressure transmitter	Deltabar S PMD75	Endress + Hauser	± 0.15 % of set span
Temperature sensor CO_2 and glycol	Class B RTD Pt100	RS PRO	± 1/3(0.3 K + 0.005*T (°C))
Mass flow meter CO_2	RHM Coriolis meter	Rheonik	± 0.2 % of reading
Volumetric flow glycol	Picomag	Endress + Hauser	± (0.8 % of reading + 0.2 % of set span)
Power meter	A9MEM3150	Schneider Electric	± 1 % of reading

Table 3
Average measurement uncertainties during experiments.

Parameters	Uncertainty	Parameters	Uncertainty
PXG LP_{in} flow	± 0.0471 kg/min	GC pressure	± 0.325 bar
PXG HP_{out} flow	± 0.0649 kg/min	PXG LP_{in} temp	± 0.175 °C
PXG HP_{in} flow	± 0.555 kg/min	PXG LP_{out} temp	± 0.130 °C
Compressor flow	± 0.415 kg/min	PXG HP_{in} temp	± 0.243 °C
LP ejector motive flow	± 0.026 kg/min	PXG HP_{out} temp	± 0.315 °C
LP ejector DP	± 0.022 bar	Ejectors motive temp	± 0.410 °C
HP ejector DP	± 0.046 bar	LP ejector suction temp	± 0.155 °C
Com discharge pressure	± 0.354 bar	HP ejector outlet temp	± 0.354 °C
Receiver pressure	± 0.017 bar		

3. Results and discussions

3.1. PXG experiments with low lift ejectors

3.1.1. Ejectors and PXG flash gas compression flow

The LP and HP ejectors are essential components for the effective functioning of the proposed configuration. The flash gas extracted from the receiver tank was directed into the LP_{in} of the PXG with the assistance of the LP ejector. The LP_{in} and HP_{out} flows must be equal, but slight mixing or thermal transport between various streams within the PXG component led to an imbalance in the flows of LP_{in} and HP_{out}. Nevertheless, manipulating the motive flows in the HP and LP ejectors can significantly reduce this disparity, thereby regulating the suction flows accordingly. The LP ejector outlet and HP ejector suction mass flow rates for four GC outlet temperatures are shown in Fig. 5. The numbers 1, 2, 3, and 4 correspond to GC temperature cases of 33 °C, 35 °C, 37 °C and 38 °C, respectively. It is evident that the outlet flow of the LP ejector exhibits a high degree of stability, whereas fluctuations are observed in the suction flow of the HP ejector. The leading cause of these oscillations can be attributed to the motive condition of the HP ejector. A slight variation in motive side pressure can impact the motive flow, perhaps leading to instability in the suction side. The regulation of travel distance within PXG is a crucial aspect that the LP and HP ejector managed. Maintaining the required travel distance can achieve a complete balance, and thermal transmission within PXG can be avoided. The average difference between LP_{in} and HP_{out} flow from case 1 to case 4 is 0.185 kg/min, 0.3 kg/min, 0.349 kg/min and 0.188 kg/min, respectively. It is observed that there is a minor degree of mixing between the inflow of HP_{in} and the outflow of high-pressure HP_{out}.

The motorised HP ejector is a distinctive device employed immediately after the compressor to elevate the pressure of the flash gas from the PXG HP outlet to the GC pressure. The HP ejector is an unconventional device that has undergone meticulous engineering and design to facilitate its manufacturing process. The attainment of the desired pressure lift and the necessary pressure differential between the ejector motive and outlet necessitates the utilisation of an HP ejector with a highly accurate geometric configuration. The HP ejector motive nozzle is the sole component responsible for regulating the compressor discharge pressure. A metering valve was built in parallel with the HP ejector to enhance safety. The valve was completely closed, as the motive nozzle of the ejector was deemed sufficient to accommodate the entire compressor flow required for an evaporation capacity of 70 kW.

3.1.2. PXG and ejectors pressure lift

The pressure difference between the HP ejector motive (Compressor discharge) and outlet (GC pressure) is shown in Fig. 6. PXG can effectively maintain the required GC pressure by adjusting the rotational speed of the PXG rotor. The PXG RPM to maintain the GC pressure was in the range of 615 to 725 for all cases. The observed maximum variation in RPM for each test condition was approximately 20.

The average pressure difference between the compressor and GC for the four cases (1 to 4) are 7.95 bar, 8.16 bar, 8.58 bar and 8.64 bar, respectively. To counteract the pressure losses within the PXG, a pressure lift of 2 bar is necessary when utilising both the LP and HP ejectors. Nevertheless, because of the unfavourable increase in compressor discharge pressure, the lift generated by the high-pressure ejector exceeds 2 bar, as shown in Fig. 7. The actual experimental system is more complex than Fig. 3 as it was designed to test various configurations and concepts. As a result, the flow from GC to PXG HP_{in} went through unwanted components, which caused an additional pressure drop of

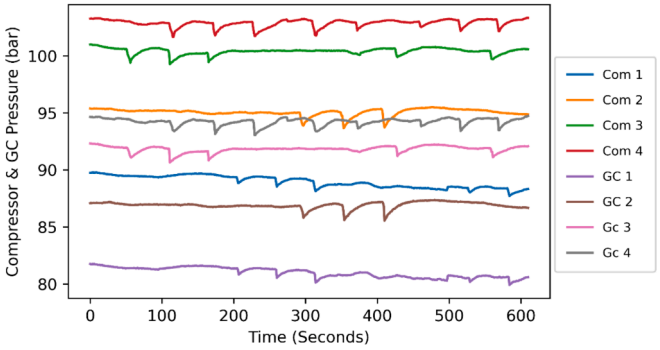

Fig. 6. Compressor discharge (Com) and GC/HP ejector outlet (GC) pressures.

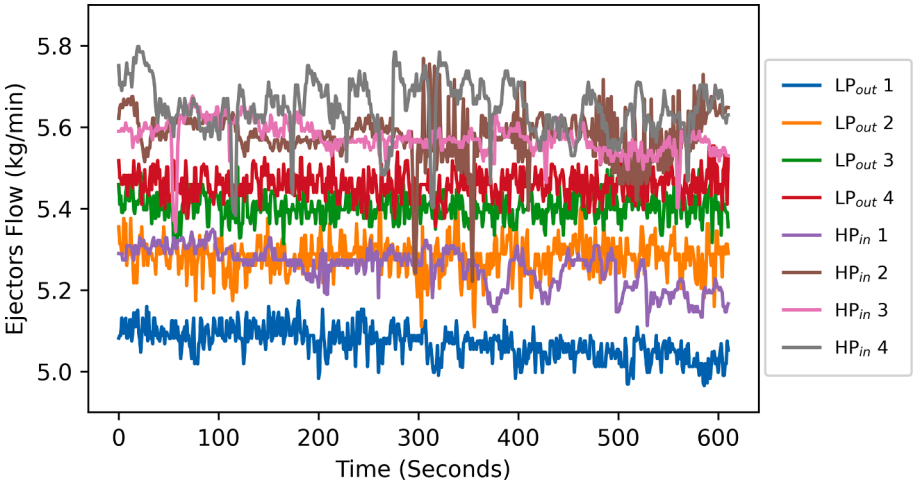

Fig. 5. LP ejector outlet and HP ejector inlet flow at various GC outlet cases.

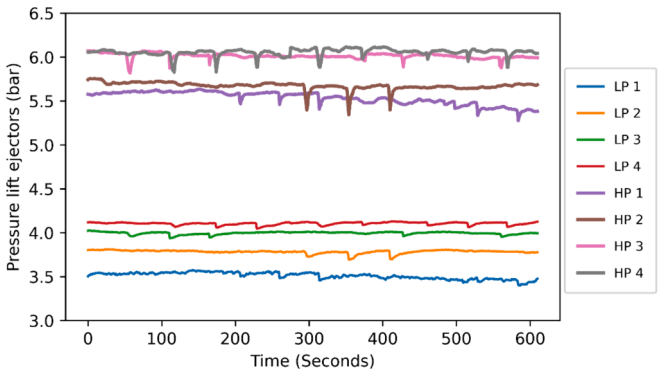

Fig. 7. LP and HP ejectors pressure lifts.

approximately 1 to 1.5 bar. This can lead to the conclusion that the current experimental system requires a pressure rise of 3 to 3.5 bar. The four cases' respective average HP ejector pressure lifts are 5.25 bar, 5.67 bar, 6.01 bar, and 6.06 bar.

LP ejector lift is closer to the design, but the challenges are there for the HP ejector. However, there was no freedom to adjust due to the fixed LP ejector motive nozzle. The experimental readings are shown in Fig. 7, and the average LP ejector pressure lift for the four cases is 3.51 bar, 3.78 bar, 3.99 bar, and 4.11 bar, respectively.

The pressure lift of flash gas from the PXG LP_{in} to HP_{out} is shown in Fig. 8. The PXG boosts the pressure of the flash gas with the recovery of expansion work from HP_{in} to LP_{out}. The average pressure lift generated by PXG in the four cases is 30.4 bar, 35.9 bar, 40.3 bar, and 42.5 bar, respectively, i.e., increasing with the increase of gas cooler outlet temperature. The LP ejector's fixed geometry resulted in a similar PXG LP_{in} flow throughout all four cases, with only a minor variation observed, limiting the PXG's work recovery potential.

3.1.3. Ejectors performance

The efficiency of the LP and HP ejectors and the entrainment ratio are depicted in Fig. 9. The entrainment ratio decreases with the decreasing ejector efficiency for both ejectors. Regarding efficiency, the LP ejector performed far better than the HP ejector, even if the latter could be regulated. The low efficiency of the HP ejectors was the primary factor contributing to the rather high-pressure difference between the compressor discharge and gas cooler (as seen in Fig. 7). This effect directly increases the compression power. Four compressors (one connected from the Parallel group) were utilised during experiments, and the total compression power for the four cases is 34 kW, 37.9 kW, 42.1 kW, and 43.8 kW, respectively. The average uncertainty of the HP and LP ejector efficiencies is ± 0.019 and ± 0.011, respectively.

The efficiency of the HP ejector plays a crucial role in determining the total performance achieved with PXG. The relationship between LP ejector efficiency and the capacity of PXG to handle flash gas is directly correlated. The higher efficiency of the LP ejector will reduce the ejector outlet flow (less motive flow) and temperature. Due to the lower temperature and flow at the ejector outlet, the density of CO_2 will increase, and the ejector can entrain more flash gas from the receiver tank, enhancing the overall performance. The temperatures at the four ports of the PX are shown in Fig. 10.

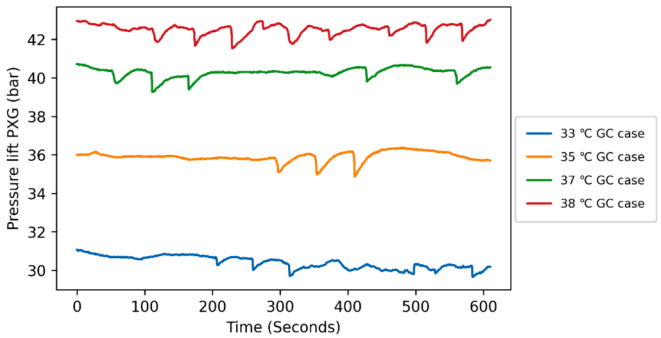

Fig. 8. PXG pressure lift of flash gas.

3.1.4. PXG expansion and vapour quality

In addition to the PXG's ability to compress the flash gas, it is imperative also to consider the expansion process. The PXG expansion pressure (Liquid receiver) was effectively controlled according to the set point. The temperature and pressure at the four ports of the PXG are known from the experiments, and three ports are equipped with flow meters as well. The vapour quality of the two-phase expanded CO_2 was calculated by the energy balance of the four ports and is shown in Fig. 11.

According to the theoretical investigation reported by Saeed et al. [32], the HP_{out} temperature should be higher than 60 °C, while experimentally, it is observed that the HP_{out} temperature was, on average, 5 °C higher than the GC outlet temperature. The temperatures at the other ports were within the range of the theoretical results. Due to this low HP_{out} temperature, the expansion vapour quality is not as low as expected but closer to the isenthalpic expansion. As highlighted earlier, the high-pressure and low-pressure travel distances must be matched precisely to have the desired effect. Due to limitations imposed by the ejectors, it was challenging to match the travel distance precisely. In any case, the free pressure lift of the flash gas achieved with PXG is a promising step towards enhanced system efficiency.

The energy savings provided by PXG slightly depend on the total system mass flow. This is because the PXG has micro-scale axial and radial gaps between its rotor and stators, which act as a hydrodynamic bearing and seal. The leakage through these gaps exerts a small efficiency debit on the PXG performance. The leakage is a function of the differential pressure between high-pressure and low-pressure ports of the PXG and the radial and circumferential distance between the high-pressure and low-pressure plenums inside the PXG, as governed by thin film flow physics (e.g., compressible form of Reynolds equation). For a given PXG geometry, the radial and circumferential distance is fixed and for a given gas cooler exit temperature, the differential pressure is fixed. Thus, the leakage flow is completely determined by the geometry and ambient temperature. Now, if the system is operated with a higher evaporator duty, the total system mass flow is larger, and the leakage flow becomes a smaller fraction of the total system mass flow, leading to a lower percentage penalty on energy savings. Thus, higher thermal duty systems are preferred for demonstrating the energy savings potential of the PXG. Additionally, since PXG controls the gas cooler pressure through its rotational speed (in lieu of the high-pressure valve of the baseline system without PXG), the higher the total system flow, the higher the PXG rotational speed. This avoids the scenarios where PXG may need to operate at very low speeds to maintain the gas cooler pressure and thus operate at sub-optimal speed. Thus, higher evaporator duty is expected to provide better PXG performance and higher energy savings.

3.2. Discussion of PXG experimental results with two booster compressors

3.2.1. PXG pressure lift

To independently confirm the findings of this study regarding the "free pressure lift" provided by the PXG and to quantify its energy savings potential in an optimal, higher evaporator duty system, a second set of experiments was carried out in a 120 kW transcritical CO_2 refrigeration system at Energy Recovery's (ERI) laboratory in San Leandro, California. The higher evaporator capacity in this system facilitates higher total system mass flows and, thus, a lower fraction of leakage flow to total system mass flow, leading to better PXG performance, as discussed above. The results from these tests are shown below.

Fig. 12 shows the "free pressure lift" provided by the PXG

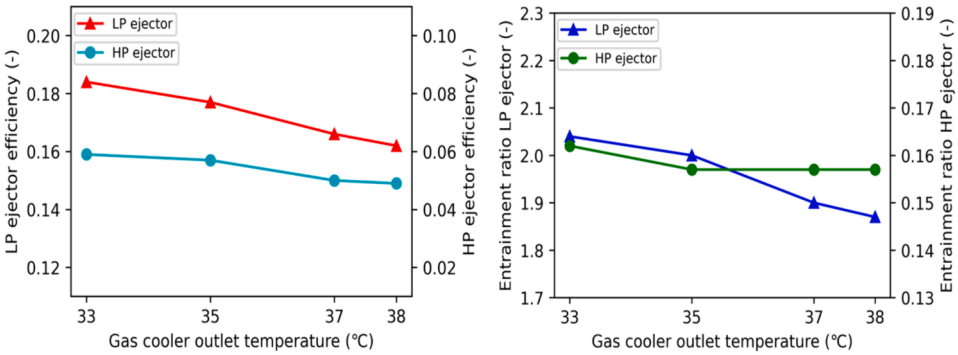

Fig. 9. LP and HP ejector efficiency (left), Entrainment ratio LP and HP ejector (right).

Fig. 10. Average temperatures measured at the four PXG ports at GC outlet 35 °C case.

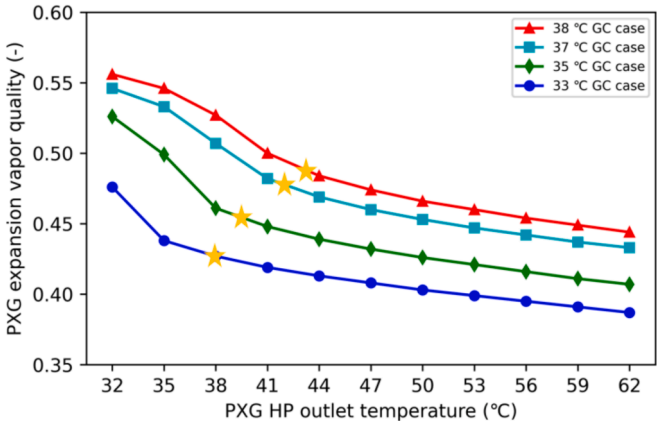

Fig. 11. PXG expansion vapour quality (Orange stars experimental points).

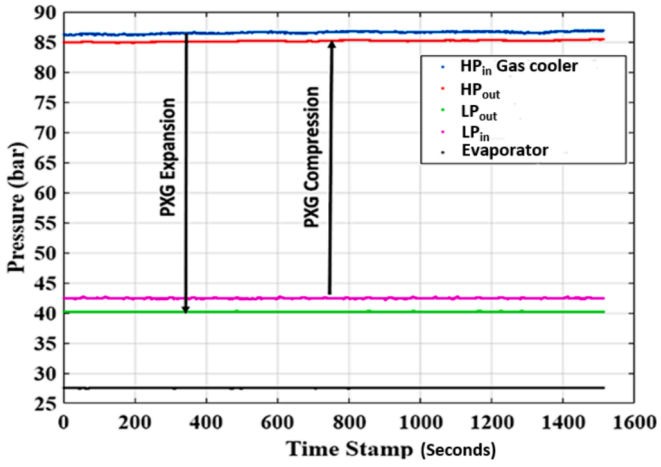

Fig. 12. Pressures measured at the four ports of the PXG during a transcritical CO_2 refrigeration test with 100 KW evaporator duty in ERI's test loop.

compression process, taking the flash gas from ~ 42 bar to 85 bar using the expansion work extracted during the PXG expansion process, which expands the supercritical CO_2 from ~ 86 bar gas cooler pressure to ~ 40 bar receiver pressure in an "isentropic-like" process. A ~ 2 bar difference between the LP_{in} pressure of the PXG and receiver pressure accounts for the viscous losses in the piping and in the PXG itself. Similarly, a ~ 1 bar difference is observed between the gas cooler exit pressure (same as PXG HPin pressure) and the PXG HPout pressure due to viscous pressure loss in the gas cooler and the PXG itself. These small pressure losses on the LP and HP side of the PXG are the reason the system architecture with low DP ejectors in series with PXG is designed and tested as discussed earlier. However, the test results at ERI confirm the significant free pressure lift (of the order of 40 + bar) provided by PXG.

3.2.2. Flows around PXG

Fig. 13 shows the mass flow rates at the four ports of the PXG during the 80–100 kW scale transcritical CO_2 refrigeration test in ERI's test loop. The results clearly show that there is very little to no "pass-through" of the compressed and expanded flow stream to the wrong side (i.e., from HP_{in} to HP_{out} and from LP_{in} to LP_{out}). Almost all the flow at LP_{in} that gets acoustically compressed inside the PXG rotor exits through the HP_{out} port as expected, and none exits through LP_{out} port. Similarly, all the flow at the high-pressure HP_{in} port that expands to low LP_{out} pressure exits through LP_{out} port, and none goes to HP_{out} port. This validates the no-pass-through characteristic of PXG operation that is desirable for an efficient PXG performance.

3.2.3. PXG performance and related parameters

Fig. 14 shows the heat absorbed and work done for a 120 kW transcritical operation with and without PXG. The evaporator load is plotted on the left vertical axis and is kept constant throughout the test. First, the system is operated in a traditional standard booster mode and consumes ~ 62 kW MT compressor work. The PXG is then brought online while maintaining the same evaporator duty and the same gas cooler exit temperature. PXG starts compressing the flash gas in the receiver using expansion work recovery, thus reducing the flash gas bypass flow going through the MT compressor. This reduces the work consumption of the MT compressor from ~ 62 kW to ~ 52 KW, as seen from the right vertical axis. Thus, PXG is able to save ~ 16 % of the work required for compression, thus increasing the COP of the system by 18.2 %.

Similar tests were conducted for a range of gas cooler exit temperatures (simulating a range of ambient temperatures) for evaporator duties in the range of 80 kW-100 kW. The results for COP improvement (COP lift) provided by PXG over a standard booster CO_2 refrigeration system are shown in Fig. 15.

As the gas cooler exit temperature increases, the density ratio (density LP_{in} / density HP_{in}) increases, as seen in Fig. 16 and thus, the mass boost ratio (MBR) that PXG is capable of achieving increases. MBR is the fraction of the total system flow that PXG can compress from LP_{in} to HP_{out} without violating the thermodynamic limits posed by the first and second laws of thermodynamics. Thus, while the baseline system becomes less and less efficient at higher gas cooler exit temperatures (i.e., lower COP), the PXG becomes capable of compressing progressively higher fractions of the total system mass flow through its free pressure lift. This progressively increases the COP lift provided by the PXG as the gas cooler exit temperature increases, as seen in Fig. 15. The anomaly at 32 °C is due to relatively flat isotherms close to the critical point, which produce large enthalpy change for a fraction of a degree of temperature change. Further, as the gas cooler pressure gets constrained at very high gas cooler exit temperatures due to safety limitations on piping and compressor discharge pressure, the amount of the flash gas produced increases rapidly, as seen in Fig. 16. The baseline system's work consumption further goes up for the same amount of heat absorbed in the evaporator compared to when the gas cooler pressure is not artificially constrained. This degrades the baseline system's COP even further; thus, the compression work saving provided by PXG becomes even more attractive.

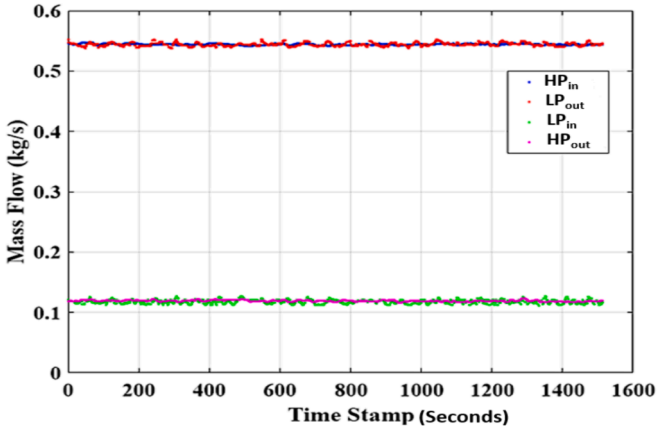

Fig. 13. Mass flows measured at the four ports of the PXG during a transcritical CO_2 refrigeration test in ERI's test loop.

Fig. 16 shows the densities and density ratio between two fluid streams entering the PXG. Since PXG is a volumetric device, the most optimal operation of PXG takes place when the available duct volume is fully utilised. This is true for both the flow coming in from LP_{in} port and filling the duct with low-pressure flash gas and for the flow coming in from HP_{in} and filling the duct with high-pressure supercritical CO_2. Since the geometry of the duct is the same in both cases, and PXG rotational speed is the same for both, the optimal volumetric flow rate for both incoming flows is the same, which is equal to the maximum volumetric flow the incoming stream can occupy without straight "pass-through". This suggests that the ratio of the two mass flows entering the PXG must be in proportion to their respective densities for the most optimal operation. This is the mass boost ratio (MBR) of the PXG. It is the ratio of the maximum LP_{in} mass flow rate that PXG can compress per unit HP_{in} mass flow rate (which is equal to the total gas cooler flow, i.e., total system mass flow). The higher the MBR, the higher the fraction of the total system flow that is compressed "for free" by the PXG, thus lowering the mass flow going through the MT compressor and, thus, lowering the work consumption of the system. As can be seen from Fig. 16, as the gas cooler exit temperature increases, the LP_{in} density remains constant (since the thermodynamic state of flash gas from the receiver is independent of the gas cooler exit temperature or pressure) however, the density of the fluid entering HP_{in} port of the PXG (same as the density of fluid at gas cooler exit) keeps on reducing, thus causing a progressive increase in the density ratio at PXG inlets (as seen from the green curve). The slope of this density ratio sharply changes at around 40 °C. This is because of the artificial constraints of gas cooler pressure (due to safety limitations as described earlier) while the gas cooler exit temperature keeps rising. This reduces the gas cooler exit density sharply and thus increases the density ratio proportionately. This increase in density ratio, in turn, increases the MBR of the PXG.

Fig. 16 also shows the calculated quality (vapour mass fraction) after expansion through the traditional high-pressure valve (HPV) of a standard booster system. It also shows the quality after the expansion of the gas cooler exit flow through the PXG, exiting the LP_{out} port of the PXG. It can be seen that under optimal conditions of "no pass-through" and low intra-duct thermal transport, the PXG produces a lower vapour mass fraction after expansion compared to HPV, which can reduce the total system mass flow required to support a given evaporator duty. This further reduces the energy consumption of the system and thus improves COP. It must be noted that such a low vapour mass fraction is not always achievable under all operating scenarios, especially due to control challenges and the requirement for PXG to utilise its rotational speed for gas cooler pressure control. However, even if the vapour mass fraction of PXG after the expansion is equal to that of HPV, the MBR of PXG

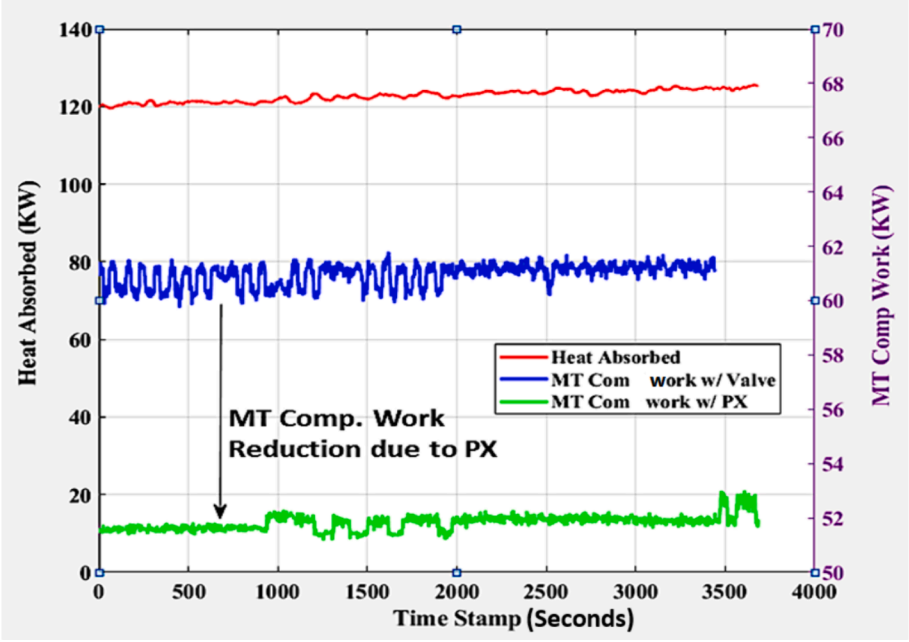

Fig. 14. Heat absorbed and work done by MT compressor as measured in transcritical CO_2 refrigeration test in ERI's test loop. The evaporator duty was held constant at 120 kW while the system was switched from a baseline system (blue line) to a PXG-based system (green line).

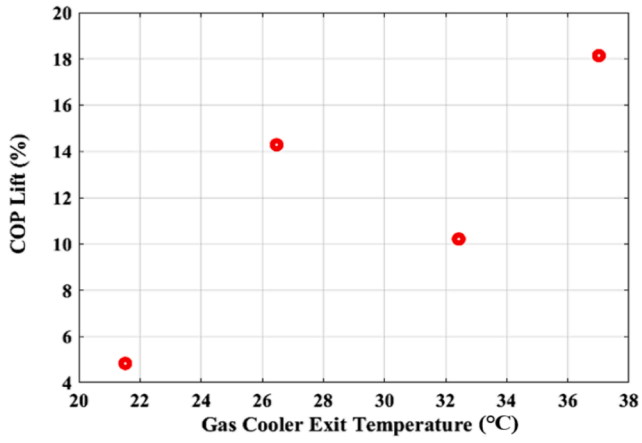

Fig. 15. COP Lift (i.e., COP improvement) provided by PXG during the transcritical CO_2 refrigeration tests in the ERI test loop.

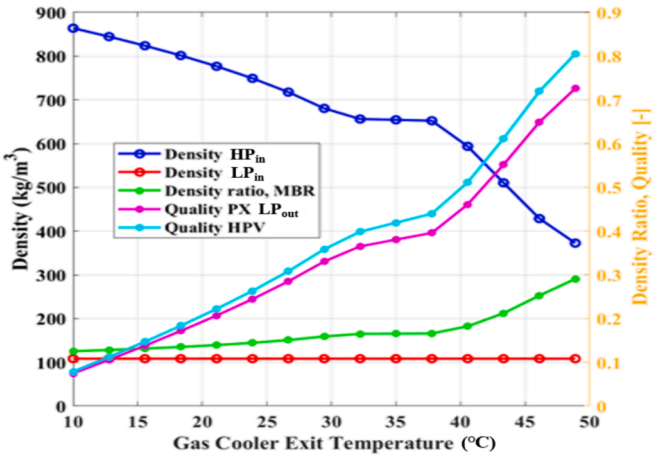

Fig. 16. Densities of two incoming streams into the PXG, their density ratio and the quality (vapour mass fraction) after the expansion through high-pressure transcritical valve (HPV) and through PXG.

provides significant enough COP improvement, as shown in Fig. 15.

4. Conclusions

The present study has experimentally validated a novel pressure exchanger integration concept for transcritical CO_2 refrigeration systems to recover the expansion work for flash gas compression. Two booster ejectors were designed and employed to enhance the functionality of PXG. The experiments were performed for the evaporation capacity of 70 kW, 0 °C evaporation temperature and GC outlet temperatures of 33 °C, 35 °C, 37 °C and 38 °C. The experimental results of the PXG system with two booster compressors are also discussed thoroughly to understand the shortcomings of testing with the new concept. The significant findings of this study are outlined as follows:

- The experimental findings have verified that the PXG can function in a setup including two booster ejectors compared to two booster compressors.
- There exists a disparity in the quantity of flash gas delivered by the LP ejector and the compressed gas extracted through the suction of the HP ejector. This disparity equals an average flow rate of 0.25 kg/min. Flow imbalance may occur when there is a lack of perfect matching between the PXG rotor's high-pressure and low-pressure travel distance.
- The average pressure difference between the compressor's discharge and the gas cooler (GC) is measured to be 8.3 bar, surpassing the intended value, resulting in increased compression work.
- The average pressure lift for the high-pressure ejector is 5.7 bar, while the low-pressure ejector has an average pressure lift of 3.8 bar.
- The flash gas compression from the LP ejector outlet pressure to the HP ejector suction pressure was successfully achieved by PXG. The average pressure lift attained for cases 1 to 4 are 30.4 bar, 35.9 bar, 40.3 bar, and 42.5 bar, respectively.
- The average efficiency of the low-pressure ejector is 17.2 %, whereas the high-pressure ejector has an average efficiency of 5.3 %. The HP

ejector needs an enhanced and more accurate design. The alteration of the motive flow was achievable by the utilisation of the motorised motive needle. However, the design of the ejector diffuser remains a primary area of focus and worry.

- On average, the output temperature of the PXG compression is approximately 5 °C higher than that of the GC. Additionally, the vapour quality during expansion is comparable to an isenthalpic expansion. Nevertheless, using PXG for free flash gas compression remains advantageous.
- Higher evaporator duty (thus higher system mass flow) tests with optimal PXG operation and higher rotational speeds have shown that PXG can provide significant free pressure lift (up to 50 bar), compressing the flash gas from receiver pressure to gas cooler pressure minus 1–2 bar pressure loss in piping and PXG itself.
- These high evaporator duty tests also demonstrated an optimal no-pass through operation of PXG, where all low-pressure flash gas went to the gas cooler inlet after compression, and all high-pressure supercritical CO_2 went to the receiver after expansion.
- Under such optimal PXG operation, PXG was able to provide up to 16 % in MT compressor work savings and up to 18.2 % in COP lift (COP improvement) compared to standard booster transcritical CO_2 system.

Declaration of competing interest

The authors declare that they have no known competing financial interests or personal relationships that could have appeared to influence the work reported in this paper.

Data availability

The authors do not have permission to share data.

Acknowledgements

The authors gratefully acknowledge the Research Council of Norway for the financial support for carrying out the present research [NFR Project No. 308779 CruiZE and Project No. 257632 HighEFF] and Energy recovery International for technical support.

References

[1] M. Nakagawa, A.R. Marasigan, T. Matsukawa, Experimental analysis on the effect of internal heat exchanger in transcritical CO2 refrigeration cycle with two-phase ejector, Int. J. Refrig. 34 (2011) 1577–1586, https://doi.org/10.1016/j.ijrefrig.2010.03.007.

[2] E. Bellos, C. Tzivanidis, A comparative study of CO2 refrigeration systems, Energy Convers. Manag.: X 1 (2019) 100002, https://doi.org/10.1016/j.ecmx.2018.100002.

[3] G. Lorentzen, Revival of carbon-dioxide as a refrigerant, Int. J. Refrig. 17 (1994) 292–301, https://doi.org/10.1016/0140-7007(94)90059-0.

[4] S. Fangtian, M. Yitai, Thermodynamic analysis of transcritical CO2 refrigeration cycle with an ejector, Appl. Therm. Eng. 31 (2011) 1184–1189, https://doi.org/10.1016/j.applthermaleng.2010.12.018.

[5] V. Sharma, B. Fricke, P. Bansal, Comparative analysis of various CO2 configurations in supermarket refrigeration systems, Int. J. Refrig. 46 (2014) 86–99, https://doi.org/10.1016/j.ijrefrig.2014.07.001.

[6] M.-H. Kim, J. Pettersen, C.W. Bullard, Fundamental process and system design issues in CO2 vapor compression systems, Prog. Energy Combust. Sci. 30 (2004) 119–174, https://doi.org/10.1016/j.pecs.2003.09.002.

[7] A.T. Diaby, P. Byrne, T. Maré, Simulation of heat pumps for simultaneous heating and cooling using CO2, Int. J. Refrig. 106 (2019) 616–627, https://doi.org/10.1016/j.ijrefrig.2019.03.010.

[8] G. Lorentzen, The use of natural refrigerants: A complete solution to the CFC/HCFC predicament, Int. J. Refrig. 18 (1995) 190–197, https://doi.org/10.1016/0140-7007(94)00001-E.

[9] M. Karampour, S. Sawalha, State-of-the-art integrated CO2 refrigeration system for supermarkets: A comparative analysis, Int. J. Refrig. 86 (2018) 239–257, https://doi.org/10.1016/j.ijrefrig.2017.11.006.

[10] A. Hafner, S. Försterling, K. Banasiak, Multi-ejector concept for R-744 supermarket refrigeration, Int. J. Refrig. 43 (2014) 1–13, https://doi.org/10.1016/j.ijrefrig.2013.10.015.

[11] C. Lucas, J. Koehler, Experimental investigation of the COP improvement of a refrigeration cycle by use of an ejector, Int. J. Refrig. 35 (2012) 1595–1603, https://doi.org/10.1016/j.ijrefrig.2012.05.010.

[12] Y. Zhu, C. Li, F. Zhang, P.-X. Jiang, Comprehensive experimental study on a transcritical CO2 ejector-expansion refrigeration system, Energ. Conver. Manage. 151 (2017) 98–106, https://doi.org/10.1016/j.enconman.2017.08.061.

[13] J.-Q. Deng, P.-X. Jiang, T. Lu, W. Lu, Particular characteristics of transcritical CO2 refrigeration cycle with an ejector, Appl. Therm. Eng. 27 (2007) 381–388, https://doi.org/10.1016/j.applthermaleng.2006.07.016.

[14] R. Llopis, L. Nebot-Andrés, R. Cabello, D. Sánchez, J. Catalán-Gil, Experimental evaluation of a CO2 transcritical refrigeration plant with dedicated mechanical subcooling, Int. J. Refrig. 69 (2016) 361–368, https://doi.org/10.1016/j.ijrefrig.2016.06.009.

[15] P. Gullo, K. Tsamos, A. Hafner, Y. Ge, S.A. Tassou, State-of-the-art technologies for transcritical R744 refrigeration systems – A theoretical assessment of energy advantages for European food retail industry, Energy Procedia 123 (2017) 46–53, https://doi.org/10.1016/j.egypro.2017.07.283.

[16] E. Söylemez, A. Hafner, C. Schlemminger, E.E. Kriezi, V. Khorshidi, The performance analysis of an integrated CO2 refrigeration system with multi-ejectors installed in a supermarket, Energies 15 (2022) 3142, https://doi.org/10.3390/en15093142.

[17] K.M. Tsamos, Y.T. Ge, I. Santosa, S.A. Tassou, G. Bianchi, Z. Mylona, Energy analysis of alternative CO2 refrigeration system configurations for retail food applications in moderate and warm climates, Energ. Conver. Manage. 150 (2017) 822–829, https://doi.org/10.1016/j.enconman.2017.03.020.

[18] N. Purohit, D.K. Gupta, M.S. Dasgupta, Energetic and economic analysis of transcritical CO2 booster system for refrigeration in warm climatic condition, Int. J. Refrig. 80 (2017) 182–196, https://doi.org/10.1016/j.ijrefrig.2017.04.023.

[19] B. Fricke, S. Zha, V. Sharma, J. Newel, Laboratory evaluation of a commercial CO2 booster refrigeration system, in: International refrigeration and air conditioning conference, Purde University, 2016.

[20] Z. Wang, H. Zhao, X. Wang, J. Han, Y. Lai, Thermodynamic performance evaluation of the CO2 parallel compression supermarket refrigeration system with a subcooler, Int. J. Energy Res. 44 (2020) 6709–6724, https://doi.org/10.1002/er.5408.

[21] J.S. Lee, M.S. Kim, M.S. Kim, Experimental study on the improvement of CO2 air conditioning system performance using an ejector, Int. J. Refrig. 34 (2011) 1614–1625, https://doi.org/10.1016/j.ijrefrig.2010.07.025.

[22] X.X. Xu, G.M. Chen, L.M. Tang, Z.J. Zhu, Experimental investigation on performance of transcritical CO2 heat pump system with ejector under optimum high-side pressure, Energy 44 (2012) 870–877, https://doi.org/10.1016/j.energy.2012.04.062.

[23] D. Li, E.A. Groll, Transcritical CO2 refrigeration cycle with ejector-expansion device, Int. J. Refrig. 28 (2005) 766–773, https://doi.org/10.1016/j.ijrefrig.2004.10.008.

[24] K. Banasiak, A. Hafner, E.E. Kriezi, K.B. Madsen, M. Birkelund, K. Fredslund, R. Olsson, Development and performance mapping of a multi-ejector expansion work recovery pack for R744 vapour compression units, Int. J. Refrig. 57 (2015) 265–276, https://doi.org/10.1016/j.ijrefrig.2015.05.016.

[25] X. Qin, Y. Zhang, D. Wang, J. Chen, System development and simulation investigation on a novel compression/ejection transcritical CO2 heat pump system for simultaneous cooling and heating, Energ. Conver. Manage. 259 (2022) 115579, https://doi.org/10.1016/j.enconman.2022.115579.

[26] G. Zhang, S. Dykas, S. Yang, X. Zhang, H. Li, J. Wang, Optimization of the primary nozzle based on a modified condensation model in a steam ejector, Appl. Therm. Eng. 171 (2020) 115090, https://doi.org/10.1016/j.applthermaleng.2020.115090.

[27] G. Zhang, S. Dykas, P. Li, H. Li, J. Wang, Accurate condensing steam flow modeling in the ejector of the solar-driven refrigeration system, Energy 212 (2020) 118690, https://doi.org/10.1016/j.energy.2020.118690.

[28] G. Zhang, Y. Li, Z. Jin, S. Dykas, X. Cai, A novel carbon dioxide capture technology (CCT) based on non-equilibrium condensation characteristics: Numerical modelling, nozzle design and structure optimisation, Energy 286 (2024) 129603, https://doi.org/10.1016/j.energy.2023.129603.

[29] Z. Guojie, L. Yunpeng, Y. Jianming, J. Zunlong, S. Dykas, Performance prediction and loss evaluation of the carbon dioxide supersonic nozzle considering the non-equilibrium condensation, J. Phys. Conf. Ser. 2707 (2024) 012009, https://doi.org/10.1088/1742-6596/2707/1/012009.

[30] K.E. Ringstad, K. Banasiak, Å. Ervik, A. Hafner, Machine learning and CFD for mapping and optimisation of CO2 ejectors, Appl. Therm. Eng. 199 (2021) 117604, https://doi.org/10.1016/j.applthermaleng.2021.117604.

[31] E.A. Groll, J.-H. Kim, Review Article: Review of Recent Advances toward Transcritical CO2 Cycle Technology, HVAC&R Research, 13 (2007) 499-520.10.1080/10789669.2007.10390968.

[32] M.Z. Saeed, Thatte A, Hafner A , Gabrielii H. C, Simultaneous implementation of rotary pressure exchanger and ejectors for CO2 refrigeration system, in: 15th IIR-Gustav Lorentzen Conference on Natural Refrigerants, 2022.https://doi.org/10.18462/iir.gl2022.0130.

[33] A. Thatte, A New Type of Rotary Liquid Piston Pump for Multi-Phase CO2 Compression, in: ASME Turbo Expo 2018: Turbomachinery Technical Conference and Exposition, Vol. Oil and Gas Applications; Supercritical CO2 Power Cycles; Wind Energy, 2018. Doi: 10.1115/GT2018-77011.

[34] A. Thatte, Transcritical / Supercritical CO2 Recompression Brayton Cycle Using a Novel Rotary Liquid Piston Compressor, in: ASME Turbo Expo 2019: Turbomachinery Technical Conference and Exposition, Vol. Oil and Gas

Applications; Supercritical CO2 Power Cycles; Wind Energy, 2019. Doi: 10.1115/gt2019-91088.
[35] Thatte A., Fricke B., Nawaz K., Novel rotary pressure exchanger for highly efficient trans-critical CO2 refrigeration cycle, in: 15th IIR-Gustav Lorentzen Conference on Natural Refrigerants, 2022.https://doi.org/10.18462/iir.gl2022.0056.
[36] A. Thatte, B. Fricke, New Types of Low Global Warming, Energy Efficient Refrigeration Architectures Using a Trans-Critical Rotary Pressure Exchanger, in: Proceedings of ASHRAE Annual Conference, TO-22-C041,Toronto, Canada, 2022.
[37] M.Z. Saeed, Á.Á. Pardiñas, K. Banasiak, A. Hafner, A. Thatte, Thermodynamic analysis of rotary pressure exchanger and ejectors for CO2 refrigeration system, Thermal Science and Engineering Progress 51 (2024) 102643, https://doi.org/10.1016/j.tsep.2024.102643.
[38] Á.Á. Pardiñas, H. Selvnes, K. Banasiak, A. Hafner, Next generation of ejector-supported R744 booster systems for commercial refrigeration at all climates, Int. J. Refrig. 148 (2023) 168–178, https://doi.org/10.1016/j.ijrefrig.2022.10.027.
[39] F. Fabris, Á.Á. Pardiñas, S. Marinetti, A. Rossetti, A. Hafner, S. Minetto, A novel R744 multi-temperature cycle for refrigerated transport applications with low-temperature ejector: Experimental ejector characterisation and thermodynamic cycle assessment, Int. J. Refrig. 152 (2023) 26–35, https://doi.org/10.1016/j.ijrefrig.2023.05.003.
[40] E. Lemmon, Huber, M., and McLinden, M., NIST standard reference database 23: Reference Fluid Thermodynamic and Transport Properties-REFPROP, Version 10.0, (2018). in.
[41] C. Aprea, F. de Rossi, R. Mastrullo, The uncertainties in measuring vapour compression plant performances, Measurement 21 (1997) 65–70, https://doi.org/10.1016/S0263-2241(97)00040-7.